Published in final edited form as:

ACS Appl Mater Interfaces. 2017 July 12; 9(27): 22259–22267. doi:10.1021/acsami.7b05664.

Nucleation and Assembly of Silica into Protein-Based Nanocomposites as Effective Anticancer Drug Carriers Using Self-Assembled Silk Protein Nanostructures as Biotemplates

Jie Wang[†], **Shuxu Yang**[‡], **Chenlin Li**[†], **Yungen Miao**[†], **Liangjun Zhu**[†], **Chuanbin Mao**[*,§,‖], and **Mingying Yang**[*,†]

[†]Institute of Applied Bioresource Research, College of Animal Science, Zhejiang University, Yuhangtang Road 866, Hangzhou 310058, China

[‡]Department of Neurosurgery, Sir Run Run Shaw Hospital, School of Medicine, Zhejiang University, Yuhangtang Road 866, Hangzhou 310058, China

[§]School of Materials Science and Engineering, Zhejiang University, Hangzhou 310027, China

[‖]Department of Chemistry & Biochemistry, Stephenson Life Science Research Center, University of Oklahoma, 101 Stephenson Parkway, Norman, Oklahoma 73019-5251, United States

Abstract

Bombyx mori (*B. mori*) silk fibroin and sericin can act as a great candidate in delivering drugs or other bioactive substances. Silica also has a great application in the field of drug delivery. To the best of our knowledge, there has been no report on the design of a nanocomposite made of silk protein and silica for drug delivery. Here, for the first time, we used *B. mori* silk fibroin (SF) and sericin (SS), self-assembled into nanospheres and nanofibers in situ in the aqueous solution, respectively, as a biotemplate to regulate the nucleation and self-assembly of silica for designing anticancer drug delivery. SF and SS mediated the nucleation and assembly of silica into monodispersed nanospheres (termed Si/SF) and nanofibers (termed Si/SS), respectively. The size and topography of the silica assemblies were dependent on the concentration of SF or SS as well as reaction conditions. Both Si/SF nanospheres and Si/SS nanofibers showed a high loading capability and sustained release profile of an anticancer drug, doxorubicin (DOX), in vitro. Si/SF nanospheres were found to be efficiently internalized in human cervical carcinoma (HeLa) cells

[*]Corresponding Authors: yangm@zju.edu.cn (M.Y.). cbmao@ou.edu (C.B.M).

ORCID

Liangjun Zhu: 0000-0001-9606-5287

Chuanbin Mao: 0000-0002-8142-3659

Notes

The authors declare no competing financial interest.

Supporting Information

The Supporting Information is available free of charge on the ACS Publications website at DOI: 10.1021/acsami.7b05664. Supplementary Figure 1: Topographies of AFM images of silk fibroin and silk sericin at various concentrations. Supplementary Figure 2: TEM image of Si/SF nanospheres after calcinations and TGA curve of Si/SF nanospheres. Supplementary Figure 3: FTIR spectra of silk protein and protein–silica nanocomposites. Supplementary Figure 4: Zeta potential distribution of silk protein, silk protein–silica nanocomposites, and synthetic silica spheres. Supplementary Figure 5: Stability analysis of Si/SF nanospheres and Si/SS nanofibers. Supplementary Figure 6: LSCM images of DOX-loaded Si/SF nanospheres and Si/SS nanofibers. Supplementary Figure 7: TEM images of Si/SF nanospheres and Si/SS nanofibers cocultured with HeLa cells for 12 h. Supplementary Figure 8: *In vitro* cytotoxicity studies of Si/SF nanospheres and Si/SS nanofibers (PDF)

and accumulate around the cell nuclei. Si/SS nanofibers could only adhere to the surface of the cancer cells. This indicates that DOX-loaded Si/SF nanospheres and Si/SS nanofibers are more Effective in cancer therapy than free DOX. Our results suggest that the self-assembled Si/SF spheres and Si/SS nanofibers are potential Effective anticancer drug carriers.

Graphical abstract

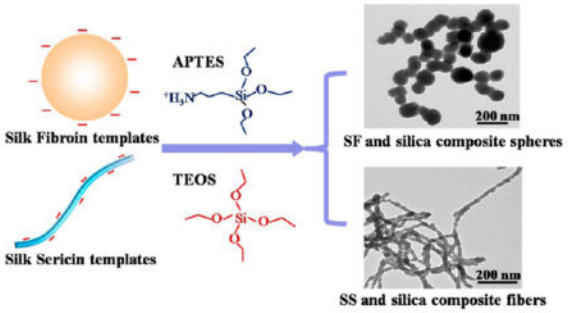

Keywords

protein; silica; nanospheres; nanofibers; drug delivery

1. INTRODUCTION

Silica nanomaterials have been extensively applied in a large variety of fields, including electronics, energy, catalysis, biology, and medicine due to their excellent electronic/mechanical properties, high surface-to-volume ratios, improved multi-functionality, as well as favorable biocompatibility.[1–4] Recently, increasing attention has been paid to silica nanomaterials for biomedical applications, especially cancer therapy, because they can act as an efficient drug carrier to transport and release drug owing to their high drug loading capacity, biocompatibility, and easy modification.[5–7] Usually, traditional anticancer drugs such as doxorubicin (DOX) molecules are easily eliminated via renal clearance or distributed in normal tissues. In contrast, silica nanomaterials can deliver anticancer drugs to the tumor, resulting in increased therapeutic efficiency.[8] For improving the performance of silica nanomaterials in drug delivery, much effort has been made to design silica in the forms of nanowires, nanofibers, or nanospheres with Different architectures such as hollow, bell-ring, or rod-like structures.[9–13]

Silk fibroin (SF) and sericin (SS) derived from the *Bombyx mori* (*B. mori*) silkworm have biocompatibility, controllable biodegradability, and excellent plasticity.[14] Both SF and SS can act as drug carriers by exhibiting high encapsulation efficacy and controllable drug release kinetics.[15–17] In addition, the acidic amino acids included in the primary structure of SF and SS can bind cations, which drives their self-assembly.[18,19] Our previous studies have used SF and SS as biotemplates to mediate the nucleation of hydroxyapatite crystals to mimic natural biomineralization.[20,21] Inspired by these findings, we hypothesized that SF and SS could be used as templates to regulate the nucleation and self-assembly of silica to

form silica/silk nanocomposites for drug delivery. To the best of our knowledge, there has been no report on the design of a nanocomposite of silk protein and silica for drug delivery.

To test our hypothesis, we first extracted aqueous SF and SS from *B. mori* silkworm cocoons. Since SF and SS have negative surface zeta potentials and abundant hydroxyl groups, we anticipated that 3-aminopropyl triethoxysilane (APTES) could interact with SS or SF through electrostatic attraction or hydrogen bonds, which in turn would trigger the nucleation and growth of silica. In addition, we speculated that the topography of biotemplates could determine the morphology of self-assembled silica and subsequent drug delivery ability. Therefore, we chose SF in the form of nanospheres and SS in the form of nanofibers as a biotemplate (Figure S1) because SF and SS tend to self-assemble into nanosphere and nanofiber in aqueous solution, respectively. Hence, as illustrated in Figure 1, APTES would be first assembled on the surface of SF nanospheres or SS nanofibers to trigger the nucleation of silica. After the addition of tetraethylorthosilicate (TEOS), the main precursor of silica, the resultant silica nuclei accelerated the hydrolysis of TEOS, leading to further silica growth. Finally, silica nanospheres and silica nanofibers mediated by SF and SS would be obtained, respectively. The drug loading and release of the resultant silica/SF nanospheres (Si/SF) and silica/SS nanofibers (Si/SS) were tested using DOX as a model anticancer drug. The cytotoxicity of Si/SF and Si/SS against human cervical carcinoma (HeLa) cells was also compared.

2. MATERIALS AND METHODS

2.1. Materials

B. mori silkworm cocoons were purchased from the Zhejiang Academy of Sericulture, China. 3-Aminopropyl triethoxysilane (APTES), tetraethylorthosilicate (TEOS), Rhodamine B isothiocyanate (RITC), fluorescein isothiocyanate (FITC), paclitaxel (PTX), and DOX were of analytical grade and purchased from Aladdin Reagents Co., Ltd. (China). Fetal bovine serum (FBS) and 0.25% trypsin were purchased from Invitrogen. Dulbecco's modified Eagle's medium (DMEM) and 1% penicillin–streptomycin were purchased from Gibco. HeLa cells were purchased from the cell bank of Chinese Academy of Sciences.

2.2. Preparation of Aqueous SF and SS Solution

An aqueous SF solution was prepared according to the previously reported procedure.[22] Briefly, small pieces of *B. mori* cocoons were boiled for 30 min in an aqueous solution with 0.5 wt % Na_2CO_3 to degum the SS. The degumming course was repeated twice. Then the degummed silk fiber was dissolved in 9.3 M LiBr solution. The solution was transferred into a dialysis bag with a molecular cutoff at 8000–14 000 Da and dialyzed against deionized water for 3 days to remove the residual salt ions. Deionized water was kept fresh during dialysis. The dialysis solution was centrifuged at 8000 rpm for 10 min to remove impurities. Finally, the supernatant was collected to form the aqueous SF solution. The concentration of SF was adjusted to the value required by experiments.

Preparation of aqueous SS solution was performed by following the reported procedure.[23] Specifically, *B. mori* cocoons were cut into small pieces, which were further washed with

deionized water to remove impurities. The washed cocoon pieces were placed into a beaker, to which 30-fold deionized water was then added. Subsequently, the beaker was heated in an autoclave with a temperature of 120 °C for 30 min to extract SS. The aqueous SS solution was generated by collecting the supernatant. After concentrated by using a rotary evaporator, the aqueous SS solution was stored at 4 °C. The SS concentration was adjusted as needed prior to use.

2.3. Silk Protein-Mediated Nucleation and Self-Assembly of Silica to Form Si/SF Nanospheres and Si/SS Nanofibers

The nucleation and self-assembly of silica mediated by SF and SS were carried out by following our earlier methods developed for other biotemplates.[24,25] Briefly, 5 mL of SF or SS solution with various concentrations (0.01, 0.1, 1, and 10 mg/mL) was precooled for 30 min in an ice–water bath. In the solution, SF or SS was self-assembled into nanospheres or nanofibers, respectively. Then, APTES with Different volumes (1, 2, and 5 μL) was dropwise added into the aqueous SF or SS solution. After gently mixed on a vortex, the reaction solution was kept in an ice–water bath for 5 min. After that, TEOS with Different volumes (5, 10, and 20 μL) was added and agitated for 3 min. The mixture solution remained in the ice–water bath for another 15 min. The resulting mixture was allowed to be aged at room temperature for 24 h. After white floccules appeared, the reaction system was centrifuged and washed with ethanol and deionized water twice each. Finally, clean specimens were obtained after being freeze-dried.

2.4. Characterization of Si/SF Nanospheres and Si/SS Nanofibers

The morphologies of the assembled silica nanocomposites were characterized using transmission electron microscopy (TEM, JEM-1200EX, JEOL) and scanning electron microscopy (SEM, SU8010, Hitachi). The samples were first resuspended with deionized water and then sonicated for 5 min to scatter the assembled silica composites. After being diluted 10 times with water, 10 μL of solution was, respectively, dropped on a silica wafer for SEM observation and on a copper grid for TEM observation. The samples were coated with gold before SEM observation and imaging. Calcination of silica nanocomposites was carried out at 550 °C for 2 h. The thermogravimetric analysis (TGA) of silica composites was measured with a thermogravimetric analyzer (DTG-60A, Shimadzu, Japan). The measurements were performed with a temperature ranging from 40 to 600 °C. The secondary structures of silica composites were measured with a Fourier transform infrared spectrometer (FTIR-8400S, Shimadzu, Japan). Before measurements, the samples were first freeze-dried for 24 h. Then, 2 mg of dried samples was mixed with 200 mg of KBr and pressed into discs. The measurements were performed with the wavenumber ranging from 400 to 4000 cm^{-1}. The surface zeta potentials of silk protein solutions before and after regulating the nucleation and self-assembly of silica were monitored and analyzed using a Nano Particle Analyzer (Zetasizer, Malvern, UK). The morphology of fresh SF and SS was characterized with atomic force microscopy (AFM, MultiMode, VEECO, U.S.A.) in tapping mode. The appearance of assembled silica nanocomposites after storage for 7 days at room temperature was recorded with a camera. The size and dispersibility of nanoparticles were monitored and analyzed using a Nano Particle Analyzer (Zetasizer, Malvern, UK).

2.5. Loading and Release of DOX by Si/SF Nanospheres and Si/SS Nanofibers in Vitro

To test the drug loading capability of silica–protein nanocomposites, we incubated Si/SF and Si/SS with DOX at various concentrations in the mixing solution. Briefly, 1 mg of lyophilized Si/SF or Si/SS was added into 2 mL of aqueous solution of DOX with a concentration ranging from 0.05 through 0.1, 0.2, 0.3, and 0.4 to 0.5 mg/mL. The mass ratio of DOX to Si/SF and Si/SS gradually increased. The mixtures were shaken in the dark for 24 h at room temperature. The products were collected by centrifugation at 6000 rpm for 5 min and washed with deionized water three times. All of the supernatants were collected. The amount of DOX in the supernatants was determined by measuring the absorbance at 490 nm using a microplate reader. The loaded drug content was calculated by using the following equation

$$\text{drug loading}\,(\%)=\frac{\text{Wd}-\text{Wr}}{\text{Ws}}\times 100\%$$

where Wd represents the total weight of DOX used in the reaction; Wr is the weight of DOX in the supernatant; and Ws is the total weight of Si/SF or Si/SS loaded with DOX.

To test DOX release, 2.5 mg of DOX-loaded Si/SF or Si/SS was added into 2 mL of phosphate-buffered saline (PBS) solution (pH 7.4) and 2 mL of acetic acid–sodium acetate (Ac–AcNa, pH 5.4) solution, respectively. At predetermined time points, 0.5 mL of buffer solution was taken out, followed by adding 0.5 mL of fresh buffer solution to keep the release system for continued drug release. The concentration of released DOX was measured by a microplate reader. Finally, the cumulative release amounts of DOX were calculated, and the release curves against time were drawn.

In addition, another anticancer drug, paclitaxel (PTX), was also used to test the loading ability of silica nanocomposite carriers. PTX is a naturally occurring anticancer drug. It can inhibit the mitosis and proliferation of tumor cells and in turn cause cell death.[26,27] Different from DOX, PTX is highly hydrophobic. We first dissolved 1 mg of PTX in 2 mL of methanol. Then 1 mg of Si/SF and Si/SS were added into PTX solution, respectively, and dispersed with an ultrasonic method. After the mixture was shaken for 24 h, the total supernatants were collected by centrifugation and washed for a few times. The concentration of PTX in the supernatant was determined by high-performance liquid chromatography (HPLC) with UV detection at 227 nm.[28] The loading efficiency of PTX in Si/SF and Si/SS was calculated by the same method as DOX.

2.6. Cellular Uptake of Si/SF Nanospheres and Si/SS Nanofibers

For investigating cellular localization of silica composites, Si/SF and Si/SS were labeled with fluorescein isothiocyanate (FITC) and rodamine B isothiocynate (RITC), respectively, following the reported procedures.[29–31] We chose HeLa cells as model cancer cells to study the cellular uptake of silica composites. The cells were cultured in DMEM and supplemented with 10% FBS and 1% penicillin-streptomycin. According to the reported procedure,[32] HeLa cells were first seeded in a 24-well plate with coverslips at 5×10^4 cells/

well to allow the cells to attach. After the cells were cultured for 24 h, the media were removed, and the cells were replenished with 1 mL of DMEM-FBS containing FITC-labeled Si/SF or RITC-labeled Si/SS (20 μg/mL). After incubation for 2 and 12 h, respectively, the media was removed and washed with PBS 3 times. Finally, the coverslips were taken out from 24-well plates and placed under a laser scanning confocal microscope (LSCM, ZEISS LSM780). Furthermore, TEM images of HeLa cells after cultured with silica particles for 12 h were observed.

2.7. In Vitro Cytotoxicity of Si/SF and Si/SS

HeLa cells were seeded in a 96-well plate at a density of 1×10^4 cells/well and cultured in 5% CO_2 at 37 °C for 24 h. To test the cytotoxicity of the silica–protein nanocomposites, Si/SF and Si/SS were added into each well with a concentration ranging from 0.1 through 0.2, 0.4, 0.8, to 1 mg/mL. In addition, the cell viability of Si/SF and Si/SS was determined by using Cell Titer 96 Aqueous One Solution cell proliferation (MTS) assay according to the manufacturer's protocol (Promega). After being cultured for 24 h, fresh culture medium was refreshed, and 20 μL of MTS was added to each well. After an additional incubation period of 4 h, the absorbance of each well was determined at 490 nm. To assess the influence of the drug release on HeLa cells, DOX-loaded Si/SF and DOX-loaded Si/SS having a DOX concentration varying from 0.2 through 0.5, 1 to 2 μg/mL were added into each well seeded with HeLa cells. Considering the sustained release of DOX, the concentration of DOX was defined as the total amounts of DOX released from carriers at an acidic environment after 7 days. Free DOX was used as a control. After cultured for 1, 2, 3, and 5 days, the cell viability of each well was determined with MTS assay.

2.8. Statistical Analysis

Data were presented as mean values ± standard deviation (SD), $n = 3$. Differences between groups were considered statistically significant at $p < 0.05$ and highly significant at $p \leq 0.01$.

3. RESULTS AND DISCUSSION

3.1. Nucleation and Self-Assembly of Silica on Silk Proteins to Form Si/SF Nanospheres and Si/SS Nano-fibers

This study aimed to utilize SF nanospheres and SS nanofibers (Figure S1) as biotemplates for regulating the nucleation and self-assembly of silica to form Si/SF nano-spheres and Si/SS nanofibers, respectively. We first determined a suitable concentration of SF and SS that can trigger the nucleation of silica. We found that SF having a concentration from 0.1 mg/mL to 10 mg/mL can form nanospheres (Figure S1) and in turn induce the nucleation and self-assembly of silica into nanospheres. As compared to the control, where the pure silica spheres (Figure 2A) having a diameter at about 500 nm were formed in the absence of SF, SF at the concentration of 0.1 mg/mL resulted in the nucleation and self-assembly of silica into Si/SF composite nanospheres with a diameter of 100 nm (Figure 2B). The diameter of Si/SF nanospheres decreased to 50 nm by increasing the concentration of SF to 1 mg/mL (Figure 2C). This is because an increase in the concentration of SF means more templates involved in triggering the nucleation and self-assembly of silica into nanospheres. Interestingly, when the concentration of SF increased to 10 mg/mL, the diameter of Si/SF

spheres increased to 200 nm (Figure 2D), probably due to the hydrogen bonding interaction between Si/SF and SF or the aggregation of SF nanospheres (Figure S1). In addition, the presence of hollow cores in the calcined Si/SF nanospheres (Figure S2) proved that SF nanospheres indeed act as a biotemplate to regulate the nucleation of silica surrounding them. TGA analysis also indicated that the Si/SF nanocomposite was composed of silica and SF, further proving that SF is present in the nanospheres (Figure S2). In the case of SS, the concentration of 0.1 and 1 mg/mL could induce the SS-templated formation of Si/SS nanofibers (Figure 2E,F). Especially, SS having a concentration of 0.1 mg/mL induced Si/SS pearl necklace-like nanofibers. We believe that an array of separated silica nuclei was first deposited on the surface of SS nanofibers, and the subsequent growth of silica nuclei on the SS nanofibers continued until neighboring growing silica domains met each other. Therefore, Figure 2 proved our hypothesis that self-assembled SF nanospheres and SS nanofibers can regulate the nucleation and self-assembly of silica into the Si/SF nanospheres and Si/SS nanofibers as illustrated in Figure 1.

Furthermore, FT-IR spectra (Figure S3) presented peaks at 1055 and 800 cm^{-1}, which can be assigned to the Si–O bond, and peaks at 1645 cm^{-1} and 1530 cm^{-1}, which are contributed by the amide I and amide II of the silk protein (SF and SS), respectively. The FT-IR data further confirmed the formation of Si/SF nanospheres and Si/SS nanofibers. The zeta potential of SF, SS, and Si/SF nanospheres and Si/SS nanofibers and control (Figure S4) supported that electrostatic attraction between SF or SS and silica plays an important role in the nucleation of silica during the formation of Si/SF spheres and Si/SS nanofibers. Furthermore, the resultant Si/SF nanospheres and Si/SS nanofibers exhibited positive zeta potential, indicating that they can load the model anticancer drug, DOX, through electrostatic attraction. In turn, the positive zeta potential prevented Si/SF nanospheres and Si/SS nanofibers from being aggregated in the buffer solution. After the solutions were stored at room temperature for 7 days, neither precipitation nor size and dispersibility change were observed (Figure S5), proving that the aqueous solutions of Si/SF nanospheres and Si/SS nanofibers are stable.

3.2. Effect of APTES and TEOS Concentration on the Morphology of Si/SF Nanospheres and Si/SS Nanofibers

APTES and TEOS are key reagents involved in the synthesis of silica.[32–35] Hence, we investigated the impact of APTES and TEOS on the morphology of Si/SF nanospheres and Si/SS nanofibers. In order to figure out whether TEOS could affect the nucleation and assembly of silica, we used SF nanospheres as a model template. The concentration of SF and the volume of APTES were fixed at 0.1 mg/mL and 5 μL, respectively, with the volume of TEOS changed from 5 μL through 10 μL to 20 μL. As shown in Figure 3, the dimension and distribution of Si/SF nanospheres were dependent on the volume of TEOS. At a condition using 5 μL of TEOS, Si/SF nanospheres appeared inhomogeneous (Figure 3A). When TEOS amount was increased to 10 μL, Si/SF nanospheres tended to be regular and bear a rough surface and a diameter of about 150 nm (Figure 3B). However, when the TEOS volume was increased to 20 μL, Si/SF nanospheres turned out to become irregular with the appearance of dot-like particles covering the surface (Figure 3C). Thus, 10 μL of TEOS might be an optimal condition for the synthesis of Si/SF nanospheres.

The conditions of APTES were optimized by using SS as a testing template. Figure 4 indicated the morphology of Si/SS nanofibers by varying the volume of APTES from 1 μL, 2 μL, to 5 μL. The TEM images showed a hollow channel inside each Si/SS nanofiber, which is the footprint of the SS nanofiber template. The silica nanoparticles are nucleated on the SS templates and then assembled along the SS templates, forming Si/SS nanofibers (Figure 4A–C). When the volume of the APTES was 1 μL, Si/SS nanofibers were short and discrete. By increasing the volume of APTES to 2 μL and 5 μL, Si/SS nanofibers tended to become longer. In particular, 5 μL of APTES resulted in the formation of bigger silica particles. SEM images (Figure 4D,E) further proved that longer nanofibers were formed with silica particles assembled on the surface in the case of using an APTES volume of 2 μL and 5 μL.

3.3. Drug Loading and Release of Si/SF Nanospheres and Si/SS Nanofibers

We selected the Si/SF nanospheres in Figure 2B and Si/SS nanofibers in Figure 4B as drug carries for testing the drug loading and release because their diameters are less than 200 nm. The drug loading efficiency gradually increased with the increase in the mass ratio of drugs and carriers, similar to other reports.[36–38] After the nanocomposites were mixed with DOX for 24 h, the highest amount of drug loaded in the Si/SF and Si/SS reached 29% and 33%, respectively (Figure 5A). Si/SF and Si/SS showed a similar drug loading capacity. This loading efficiency was much higher than that for the reported drug delivery systems based on silica nanoparticles (mostly less than 10%)[39–42] and silk protein drug carriers.[43,44] Furthermore, we found that the amount of hydrophobic drug, PTX, loaded in the Si/SF and Si/SS reached 7.03 ± 0.9% and 8.45 ± 0.8%, respectively. The loading efficiency was also higher than that for the conventional hydrophobic drug delivery agents.[45–47] The results indicated Si/SF nanospheres and Si/SS nanofibers can load either hydrophilic or hydrophobic anticancer drugs. This might be attributed to the dual drug delivery abilities of silk proteins and large surface area of nanocomposite silica spheres and fibers.

Furthermore, LSCM images showed Si/SF nanospheres and Si/SS nanofibers labeled with FITC-emitted green fluorescence (Figure S6). After loading with DOX that has red fluorescence, fluorescence was changed to be yellow, further proving that DOX can be successfully loaded into Si/SF nanospheres and Si/SS nanofibers.

In addition, DOX release was tested in a buffered solution of two Different pH values (7.4 and 5.4). Figure 5 showed a burst release of DOX from Si/SF and Si/SS at the initial stage at pH 5.4. In contrast, Si/SF nanospheres and Si/SS nanofibers showed a slow release sustained at pH 7.4 up to 1 week. After 1 week, both Si/SF nanospheres and Si/SS nanofibers released nearly 75% of loaded DOX at pH 5.4. However, they released only 20% of loaded DOX at pH 7.4. We assumed that a condition of pH 5.4 induced the disruption of electrostatic attraction between DOX and its carrier (Si/SF nanospheres or Si/SS nanofibers), which further leads to the burst release of DOX. However, a condition of pH 7.4 did not favor such disruption and thus resulted in a less Effective release. This means that Si/SF and Si/SS can Effectively release drug in treating cancer because the tumor microenvironment is acidic with a pH value close to 5.4. Interestingly, Si/SF spheres and Si/SS nanofibers demonstrated a similar DOX release profile.

3.4. Cellular Uptake of Si/SF Nanospheres and Si/SS Nanofibers

We used FITC-labeled Si/SF nanospheres and RITC-labeled Si/SS nanofibers to coculture with HeLa cells for investigating the cell uptake and localization of drug carriers. As shown in Figure 6, after the cells were cultured for 2 h, few Si/SF nanospheres entered the cells. By a culture time of 12 h, most Si/SF spheres crossed the cell membrane and accumulated around the cell nuclei. In contrast to Si/SF nanospheres, Si/SS nanofibers only gathered outside the cells without the occurrence of cellular uptake. TEM images further proved that only Si/SF spheres entered HeLa cells, as evidenced by the appearance of black particles and pores inside the cells (Figure S7). Accumulation of the Si/SF nanospheres inside the HeLa cells is similar to that reported for the silica nanospheres.[48] We assumed that the fibrous structure of Si/SS nanofibers prevented them from penetrating the cell membrane. Therefore, we supposed that Si/SF nanospheres could release DOX inside the cells, whereas Si/SS nanofibers adhered to the cellular membrane due to interaction of their positive surface charge.

3.5. In Vitro Cytotoxicity Assay

Prior to DOX loading, the cytotoxicity of Si/SF nanospheres and Si/SS nanofibers was investigated. As shown in Figure S8, after incubated for 24 h, HeLa cells cocultured with the Si/SF nanospheres and Si/SS nanofibers at a concentration of 1 mg/mL exhibited a viability higher than 70% compared with the control. This indicated that the IC50 of Si/SF nanospheres and Si/SS nanofibers in HeLa cells is over 1 mg/mL, ensuring that the Si/SF nanospheres and Si/SS nanofibers are biocompatible and thus suitable to serve as a drug carrier.

After DOX was loaded, MTS assay was performed to evaluate whether DOX released from the Si/SF nanospheres and Si/SS nanofibers could inhibit the growth of HeLa cells. As shown in Figure 7, when the concentration of DOX loaded by Si/SF nanospheres and Si/SS nanofibers is as high as 2 μg/mL, DOX-loaded Si/SF nanospheres and DOX-loaded Si/SS nanofibers as well as free DOX control showed no significant Difference on the cell viability. After the cells were cultured for 1 day, free DOX killed HeLa cells faster than DOX-loaded Si/SF nanospheres and DOX-loaded Si/SS nanofibers due to the sustained release of DOX from Si/SF nanospheres and Si/SS nanofibers. After the cells were cultured for 2 days, most of the HeLa cells were killed, indicating that the concentration of 2 μg/mL is the lethal dose for HeLa cells within a short time. When the concentration of DOX was decreased to 1 and 0.5 μg/mL, respectively, DOX-loaded Si/SF nanospheres showed a faster rate in inhibiting HeLa cells than free DOX and DOX-loaded Si/SS nanofibers after cultured for 1 day. When the concentration of DOX was decreased to 0.2 μg/mL, there existed a significant Difference in inhibiting HeLa cells between the control group (free DOX) and the experimental groups (DOX-loaded Si/SF nanospheres and Si/SS nanofibers) at Different culture time points (1, 2, and 3 days). The experiment groups showed a lower cell viability than the control group, indicating that DOX loaded in Si/SF nanospheres and Si/SS nanofibers can more efficiently kill HeLa cells than free DOX. This is because DOX-loaded Si/SF nanospheres and Si/SS nanofibers can easily reach tumor cells due to the positively charged surface, followed by sustained DOX release.

4. CONCLUSIONS

In order to develop a new anticancer drug delivery system, this study successfully employed self-assembled SF nanospheres and SS nanofibers as a biotemplate to regulate the nucleation of self-assembly of silica. We found that SF and SS mediated the nucleation and assembly of silica into monodispersed nanospheres and nanofibers, respectively. The size and topography of silica assemblies were controlled by the concentration of SF or SS and reaction conditions. FTIR and zeta potential analysis proved that the nucleation on the silk proteins was induced by the hydrolysis of APTES, and the subsequent self-assembly of silica was promoted by hydrogen bonding or electrostatic attraction between the silica and the silk proteins. The resultant self-assembled Si/SF nanospheres and Si/SS nanofibers both showed a high drug loading capability for hydrophilic DOX and hydrophobic PTX. Si/SF nanospheres and Si/SS nanofibers presented a burst release of DOX at pH 5.4 but kept slow release at pH 7.4 in vitro. Si/SF spheres could efficiently enter the cells and accumulated around the cell nuclei, but Si/SS nanofibers only adhered to the surface of the cells. Therefore, DOX-loaded Si/SF nanospheres and DOX-loaded Si/SS nanofibers have higher cytotoxicity against HeLa cells than free DOX. Our work suggested that the nanocomposites generated by silk protein mediated nucleation and self-assembly of silica are a promising drug carrier in cancer therapy.

Supplementary Material

Refer to Web version on PubMed Central for supplementary material.

Acknowledgments

We acknowledge the support of Zhejiang Provincial Natural Science Foundation of China (LZ17C170002 and LZ16E030001), Natural Science Foundation of China (51673168), State of Sericulture Industry Technology System (CARS-22-ZJ0402), and National High Technology Research and Development Program 863 (2013AA102507). CBM would also like to thank the financial support from National Institutes of Health (CA195607), Oklahoma Center for Adult Stem Cell Research (434003), and Oklahoma Center for the Advancement of Science and Technology (HR14-160).

References

1. He Y, Fan CH, Lee ST. Silicon Nanostructures for Bioapplications. Nano Today. 2010; 5:282–295.
2. Ding Z, Quinn BM, Haram SK, Pell LE, Korgel BA, Bard AJ. Electrochemistry and Electrogenerated Chemiluminescence from Silicon Nanocrystal Quantum Dots. Science. 2002; 296:1293–1297. [PubMed: 12016309]
3. Allen JE, Hemesath ER, Perea DE, Lensch-Falk JL, Li ZY, Yin F, Gass MH, Wang P, Bleloch AL, Palmer RE, Lauhon LJ. High-Resolution Detection of Au Catalyst Atoms in Si Nanowires. Nat Nanotechnol. 2008; 3:168–173. [PubMed: 18654490]
4. Pavesi L, Dal Negro L, Mazzoleni C, Franzo G, Priolo F. Optical Gain in Silicon Nanocrystals. Nature. 2000; 408:440–444. [PubMed: 11100719]
5. Trewyn BG, Giri S, Slowing II, Lin VSY. Mesoporous Silica Nanoparticle Based Controlled Release, Drug Delivery, and Biosensor Systems. Chem Commun. 2007; 31:3236–3245.
6. Slowing II, Vivero-Escoto JL, Wu CW, Lin VSY. Mesoporous Silica Nanoparticles as Controlled Release Drug Delivery and Gene Transfection Carriers. Adv Drug Delivery Rev. 2008; 60:1278–1288.
7. Bae SW, Tan WH, Hong JI. Fluorescent Dye-Doped Silica Nanoparticles: New Tools for Bioapplications. Chem Commun. 2012; 48:2270–2282.

8. Peng F, Su YY, Zhong YL, Fan CH, Lee ST, He Y. Silicon Nanomaterials Platform for Bioimaging, Biosensing, and Cancer Therapy. Acc Chem Res. 2014; 47:612–623. [PubMed: 24397270]
9. Peng F, Su YY, Wei XP, Lu YM, Zhou YF, Zhong YL, Lee ST, He Y. Silicon-Nanowire-Based Nanocarriers with Ultrahigh Drug-Loading Capacity for In Vitro and In Vivo Cancer Therapy. Angew Chem, Int Ed. 2013; 52:1457–1461.
10. Jin RH, Yuan JJ. Shaped Silicas Transcribed from Aggregates of Four-Armed Star Polyethyleneimine with a Benzene Core. Chem Mater. 2006; 18:3390–3396.
11. Beck JS, Vartuli JC, Roth WJ, Leonowicz ME, Kresge CT, Schmitt KD, Chu CTW, Olson DH, Sheppard EW, Mccullen SB, Higgins JB, Schlenker JL. A New Family of Mesoporous Molecular-Sieves Prepared with Liquid-Crystal Templates. J Am Chem Soc. 1992; 114:10834–10843.
12. Lou XW, Archer LA, Yang ZC. Hollow Micro-/Nanostructures: Synthesis and Applications. Adv Mater. 2008; 20:3987–4019.
13. Liu J, Qiao SZ, Chen JS, Lou XW, Xing XR, Lu GQ. Yolk/Shell Nanoparticles: New Platforms for Nanoreactors, Drug Delivery and Lithium-Ion Batteries. Chem Commun. 2011; 47:12578–12591.
14. Vepari C, Kaplan DL. Silk as a Biomaterial. Prog Polym Sci. 2007; 32:991–1007. [PubMed: 19543442]
15. Coburn JM, Na E, Kaplan DL. Modulation of Vincristine and Doxorubicin Binding and Release from Silk Films. J Controlled Release. 2015; 220:229–238.
16. Guziewicz N, Best A, Perez-Ramirez B, Kaplan DL. Lyophilized Silk Fibroin Hydrogels for the Sustained Local Delivery of Therapeutic Monoclonal Antibodies. Biomaterials. 2011; 32:2642–2650. [PubMed: 21216004]
17. Wenk E, Wandrey AJ, Merkle HP, Meinel L. Silk Fibroin Spheres as a Platform for Controlled Drug Delivery. J Controlled Release. 2008; 132:26–34.
18. Hardy JG, Scheibel TR. Composite Materials Based on Silk Proteins. Prog Polym Sci. 2010; 35:1093–1115.
19. Wang XQ, Yucel T, Lu Q, Hu X, Kaplan DL. Silk Nanospheres and Microspheres from Silk/Pva Blend Films for Drug Delivery. Biomaterials. 2010; 31:1025–1035. [PubMed: 19945157]
20. Yang MY, He W, Shuai YJ, Min SJ, Zhu LJ. Nucleation of Hydroxyapatite Crystals by Self-Assembled Bombyx mori Silk Fibroin. J Polym Sci, Part B: Polym Phys. 2013; 51:742–748.
21. Yang MY, Shuai YJ, Zhang C, Chen YY, Zhu LJ, Mao CB, OuYang HW. Biomimetic Nucleation of Hydroxyapatite Crystals Mediated by Antheraea pernyi Silk Sericin Promotes Osteogenic Differentiation of Human Bone Marrow Derived Mesenchymal Stem Cells. Biomacromolecules. 2014; 15:1185–1193. [PubMed: 24666022]
22. Min SJ, Gao X, Han CM, Chen Y, Yang MY, Zhu LJ, Zhang HP, Liu L, Yao JM. Preparation of a Silk Fibroin Spongy Wound Dressing and Its Therapeutic Efficiency in Skin Defects. J Biomater Sci, Polym Ed. 2012; 23:97–110. [PubMed: 21176393]
23. Wu JH, Wang Z, Xu SY. Preparation and Characterization of Sericin Powder Extracted from Silk Industry Wastewater. Food Chem. 2007; 103:1255–1262.
24. Wang FK, Nimmo SL, Cao BR, Mao CB. Oxide Formation on Biological Nanostructures Via a Structure-Directing Agent: Towards an Understanding of Precise Structural Transcription. Chem Sci. 2012; 3:2639–2645. [PubMed: 23630644]
25. Li D, Zhu Y, Mao CB. One-Pot Synthesis of Surface Roughness Controlled Hollow Silica Spheres with Enhanced Drug Loading and Release Profiles under Ambient Conditions in Aqueous Solutions. J Mater Chem B. 2013; 1:5515–5520.
26. Wani MC, Taylor HL, Wall ME, Coggon P, McPhail AT. Plant Antitumor Agents. VI. Isolation and Structure of Taxol, a Novel Antileukemic and Antitumor Agent from Taxus Brevifolia. J Am Chem Soc. 1971; 93:2325–2327. [PubMed: 5553076]
27. Holmes FA, Walters RS, Theriault RL, Forman AD, Newton LK, Raber MN, Buzdar AU, Frye DK, Hortobagyi GN. Phase II Trial of Taxol, An Active Drug in The Treatment of Metastatic Breast Cancer. J Natl Cancer Inst. 1991; 83:1797–1805. [PubMed: 1683908]
28. Fonseca C, Simoes S, Gaspar R. Paclitaxel-Loaded PLGA Nanoparticles: Preparation, Physicochemical Characterization and In Vitro Anti-Tumoral Activity. J Controlled Release. 2002; 83:273–286.

29. Baumgartel T, von Borczyskowski C, Graaf H. Selective Surface Modification of Lithographic Silica Oxide Nanostructures by Organofunctional Silanes. Beilstein J Nanotechnol. 2013; 4:218–226. [PubMed: 23616941]
30. Imhof A, Megens M, Engelberts JJ, de Lang DTN, Sprik R, Vos WL. Spectroscopy of Fluorescein (FITC) Dyed Colloidal Silica Spheres. J Phys Chem B. 1999; 103:1408–1415.
31. Wang JP, Sun JH, Li YZ, Wang F. Preparation, Characterization and Luminescent Properties of Dense Nano-Silica Hybrids Loaded with 1: 8-Naphthalic Anhydride. Luminescence. 2014; 29:188–194. [PubMed: 23765586]
32. Wang SH, Xu T, Yang YH, Shao ZZ. Colloidal Stability of Silk Fibroin Nanoparticles Coated with Cationic Polymer for Effective Drug Delivery. ACS Appl Mater Interfaces. 2015; 7:21254–21262. [PubMed: 26331584]
33. Wang FK, Li D, Mao CB. Genetically Modifiable Flagella as Templates for Silica Fibers: From Hybrid Nanotubes to 1D Periodic Nanohole Arrays. Adv Funct Mater. 2008; 18:4007–4013.
34. Van Bommel KJC, Shinkai S. Silica Transcription in the Absence of a Solution Catalyst: The Surface Mechanism. Langmuir. 2002; 18:4544–4548.
35. Monnier A, Schuth F, Huo Q, Kumar D, Margolese D, Maxwell RS, Stucky GD, Krishnamurty M, Petroff P, Firouzi A, Janicke M, Chmelka BF. Cooperative Formation of Inorganic-Organic Interfaces in The Synthesis of Silicate Mesostructures. Science. 1993; 261:1299–1303. [PubMed: 17731857]
36. Fan XJ, Jiao GZ, Zhao W, Jin PF, Li X. Magnetic $Feffo_4$–Graphene Composites as Targeted Drug Nanocarriers for pH-Activated Release. Nanoscale. 2013; 5:1143–1152. [PubMed: 23288110]
37. Yang XY, Zhang XY, Ma YF, Huang Y, Wang YS, Chen YS. Superparamagnetic Graphene Oxide–$Feffo_4$ Nanoparticles Hybrid for Controlled Targeted Drug Carriers. J Mater Chem. 2009; 19:2710–2714.
38. Zhang LM, Xia JG, Zhao QH, Liu LW, Zhang ZJ. Functional Graphene Oxide as a Nanocarrier for Controlled Loading and Targeted Delivery of Mixed Anticancer Drugs. Small. 2010; 6:537–544. [PubMed: 20033930]
39. He XX, Hai L, Su J, Wang KM, Wu X. One-pot Synthesis of Sustained-Released Doxorubicin Silica Nanoparticles for Aptamer Targeted Delivery to Tumor Cells. Nanoscale. 2011; 3:2936–2942. [PubMed: 21623439]
40. Yuan H, Bao X, Du YZ, You J, Hu FQ. Preparation and Evaluation of SiO_2-Deposited Stearic Acid-g-Chitosan Nanoparticles for Doxorubicin Delivery. Int J Nanomed. 2012; 7:5119–5128.
41. Compagnin C, Bàu L, Mognato M, Celotti L, Miotto G, Arduini M, Moret F, Fede C, Selvestrel F, Echevarria IMR, Mancin F, Reddi Elena. The Cellular Uptake of Meta-Tetra (Hydroxyphenyl) Chlorin Entrapped in Organically Modified Silica Nanoparticles is Mediated by Serum Proteins. Nanotechnology. 2009; 20:345101. [PubMed: 19652275]
42. Li L, Gu Z, Gu WY, Liu J, Xu ZP. Efficient Drug Delivery using SiO_2-Layered Double Hydroxide Nanocomposites. J Colloid Interface Sci. 2016; 470:47–55. [PubMed: 26930539]
43. Lammel AS, Hu X, Park SH, Kaplan DL, Scheibel TR. Controlling Silk Fibroin Particle Features for Drug Delivery. Biomaterials. 2010; 31:4583–4591. [PubMed: 20219241]
44. Xia XX, Wang M, Lin YN, Xu QB, Kaplan DL. Hydrophobic Drug-Triggered Self-Assembly of Nanoparticles from Silk-Elastin-Like Protein Polymers for Drug Delivery. Biomacromolecules. 2014; 15:908–914. [PubMed: 24527851]
45. Zhang XG, Miao J, Dai YQ, Du YZ, Yuan H, Hu FQ. Reversal Activity of Nanostructured Lipid Carriers Loading Cytotoxic Drug in Multi-Drug Resistant Cancer Cells. Int J Pharm. 2008; 361:239–244. [PubMed: 18586075]
46. Zhang P, Lu JQ, Huang YX, Zhao WC, Zhang YF, Zhang XL, Li J, Venkataramanan R, Gang X, Li S. Design and Evaluation of a PEGylated Lipopeptide Equipped with Drug-Interactive Motifs as an Improved Drug Carrier. AAPS J. 2014; 16:114–124. [PubMed: 24281690]
47. Miao J, Du YZ, Yuan H, Zhang XG, Li Q, Rao YF, Zhao MD, Hu FQ. Improved Cytotoxicity of Paclitaxel Loaded in Nanosized Lipid Carriers by Intracellular Delivery. J Nanopart Res. 2015; 17:1–13.

48. Gyenge EB, Darphin X, Wirth A, Pieles U, Walt H, Bredell M, Maake C. Uptake and Fate of Surface Modified Silica Nanoparticles in Head and Neck Squamous Cell Carcinoma. J Nanobiotechnol. 2011; 9:32.

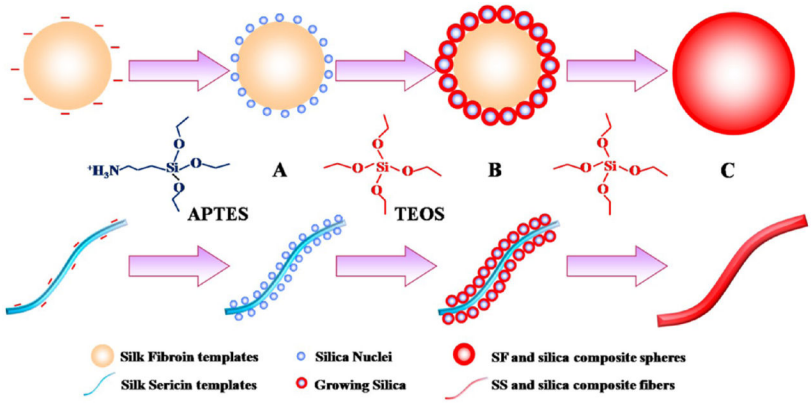

Figure 1.

Proposed schematic describing the nucleation and self-assembly of silica into nanocomposites regulated by self-assembled SF nanospheres and SS nanofibers. (A) APTES was first added into SF (top) and SS (bottom) solution to form an array of tiny silica nuclei on the surface of SF nanospheres (top) and SS nanofibers (bottom) assembled in the solution, respectively. (B) TEOS was subsequently added into the corresponding solution, and its hydrolysis resulted in the formation of silica on the silica nuclei to induce silica growth on the SF nanospheres (top) and SS nanofibers (bottom). (C) With the addition of more TEOS, continuous growth of silica on the SF nanospheres (top) and SS nanofibers (bottom) gave rise to spherical (top) and fibrous (bottom) silica nanocomposites, respectively.

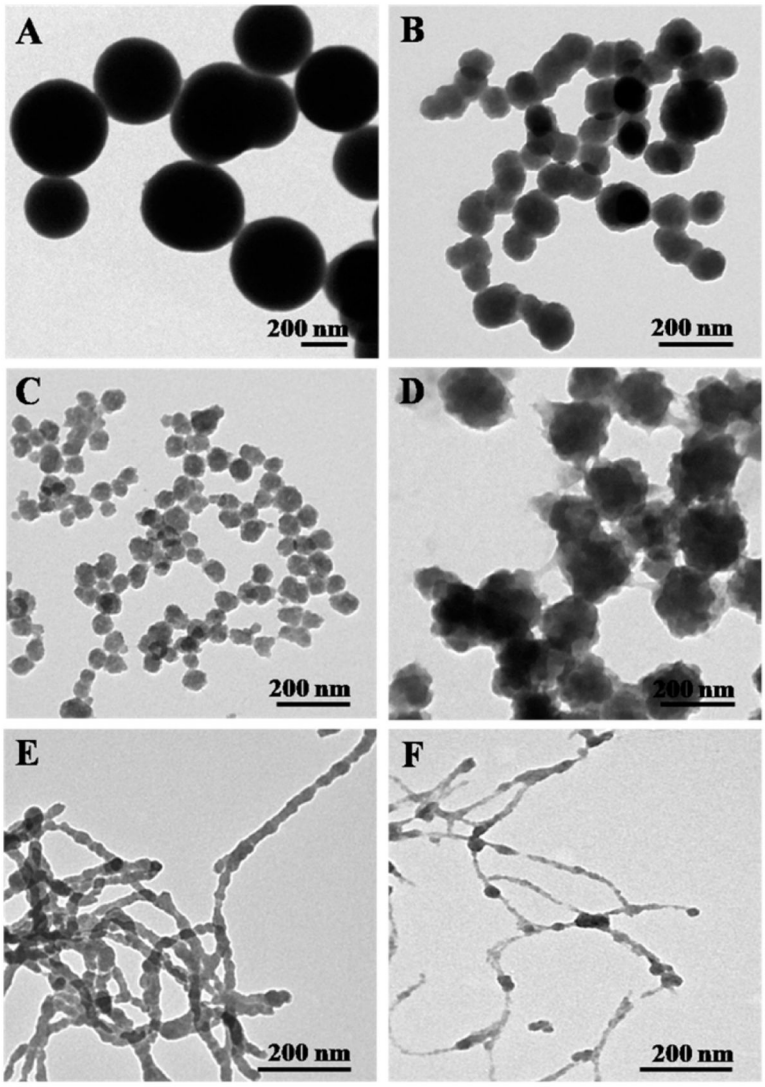

Figure 2.

TEM images showing the nucleation and self-assembly of silica into nanocomposites regulated by SF and SS with Different concentrations. (A–D) The concentration of SF was set at (A) 0, (B) 0.1, (C) 1, and (D) 10 mg/mL. (E,F) The concentration of SS was set at (E) 0.1 and (F) 1 mg/mL. During the regulating course, the amounts of APTES and TEOS were 5 μL and 10 μL, respectively.

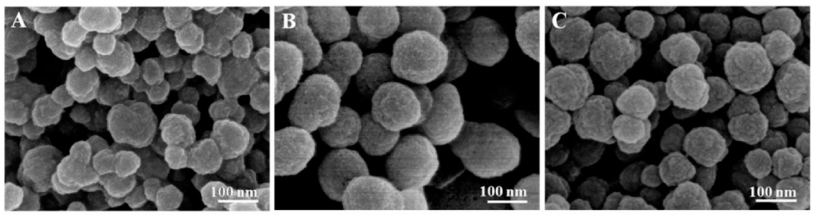

Figure 3.

SEM images confirming the nucleation and self-assembly of silica into nanospheres regulated by SF at various amounts of TEOS. The amount of TEOS was set at (A) 5, (B) 10, and (C) 20 μL. The concentration of SF and the amount of APTES were fixed on 0.1 mg/mL and 5 μL, respectively.

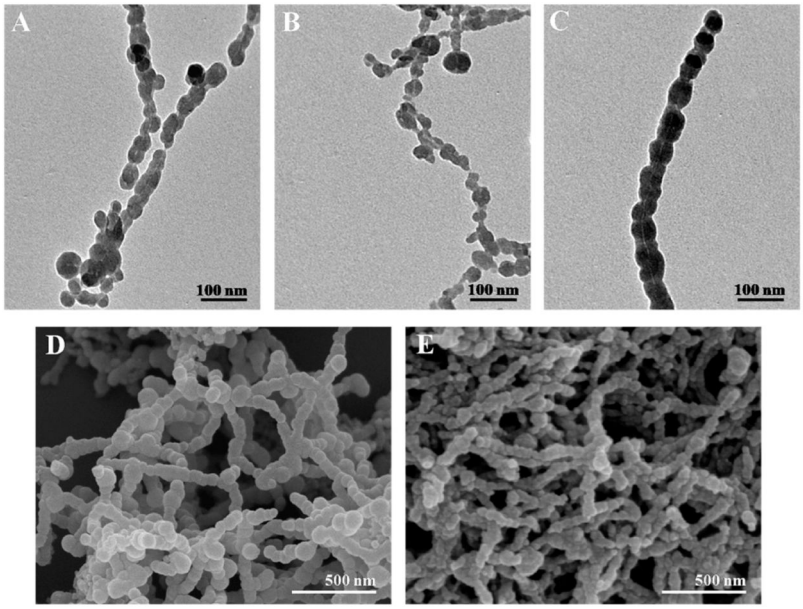

Figure 4.

TEM and SEM images showing the nucleation and assembly of silica into Si/SS nanofibers regulated by SS at various amounts of APTES. (A–C) TEM images of Si/SS nanofibers when the amount of APTES was set at (A) 1, (B) 2, and (C) 5 μL. (D,E) Corresponding SEM images of Si/SS nanofibers when the amount of APTES used was (D) 2 μL and (E) 5 μL. The concentration of SS and the amount of TEOS were fixed on 0.1 mg/mL and 10 μL, respectively.

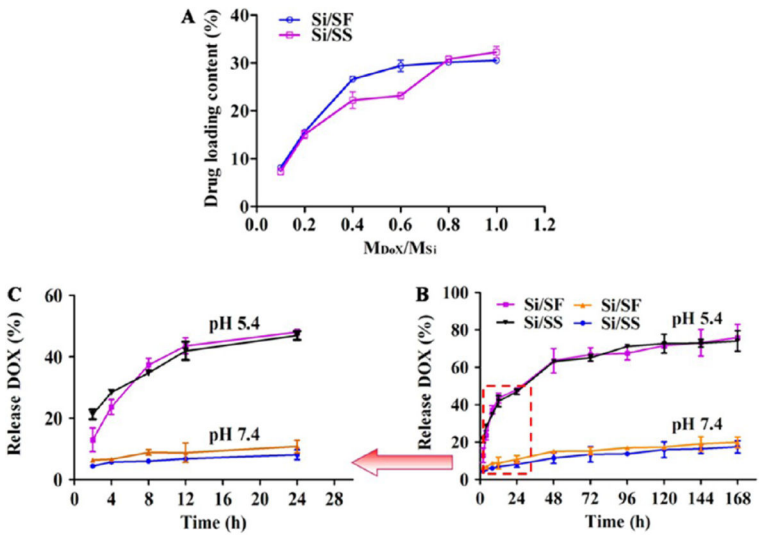

Figure 5.

In vitro DOX drug loading and release curves of Si/SF nanospheres and Si/SS nanofibers. (A) Drug loading content in the Si/SF nanospheres and Si/SS nanofibers was varied when the nanocomposites were treated with Different amounts of DOX (represented by the molar ratio between DOX and Si). (B) Drug release profile of DOX-loaded Si/SF nanospheres and Si/SS nanofibers under pH 5.4 and pH 7.4. (C) Magnified image of the dashed box region in B.

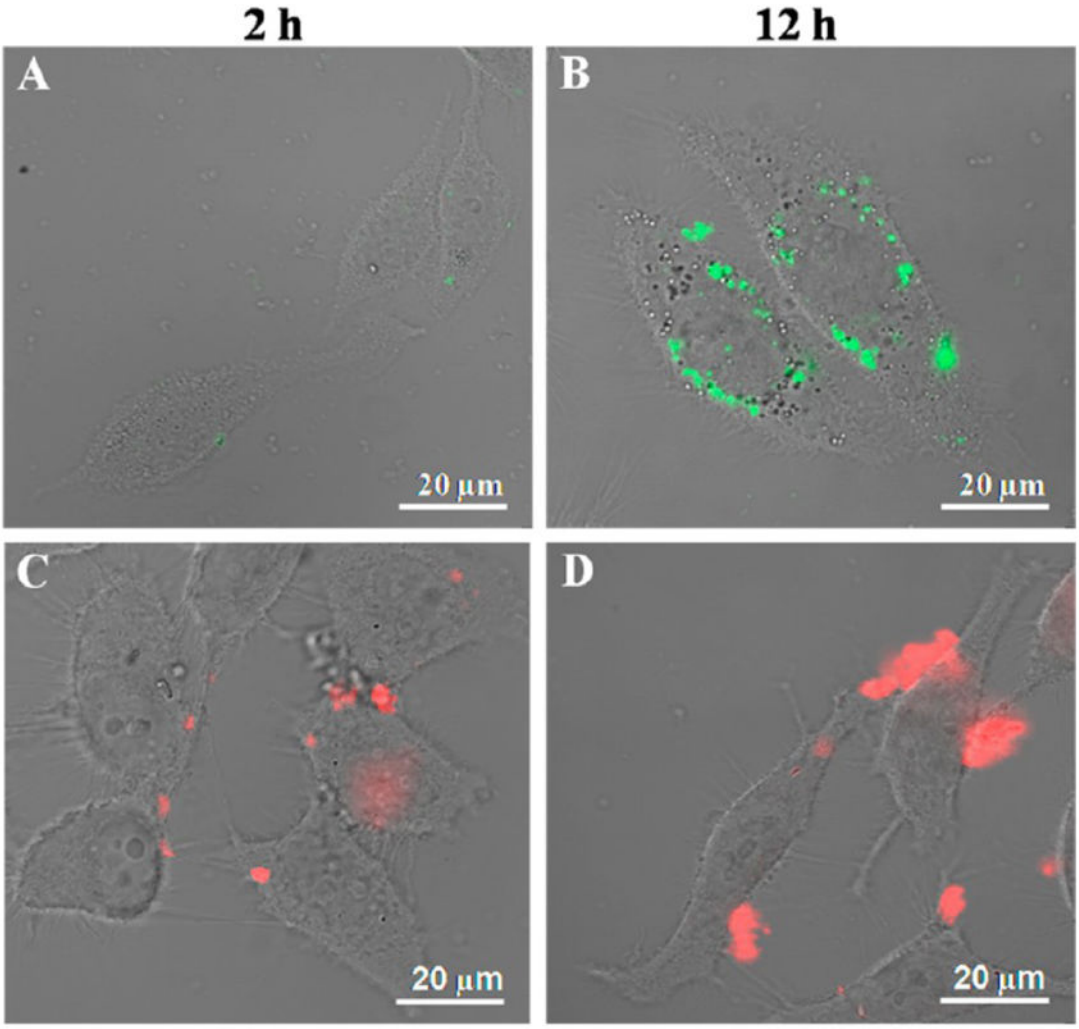

Figure 6.

LSCM images of Si/SF nanospheres and Si/SS nanofibers in HeLa cells at 37 °C under an atmosphere of 5% CO_2. HeLa cells were cocultured with Si/SF (A, B) and Si/SS (C, D) for 2 or 12 h, respectively. Si/SF nanospheres were labeled with FITC that was excited by 495 nm laser to emit green fluorescence, while Si/SS nanofibers were labeled with RITC that was excited by 565 nm laser to emit red fluorescence.

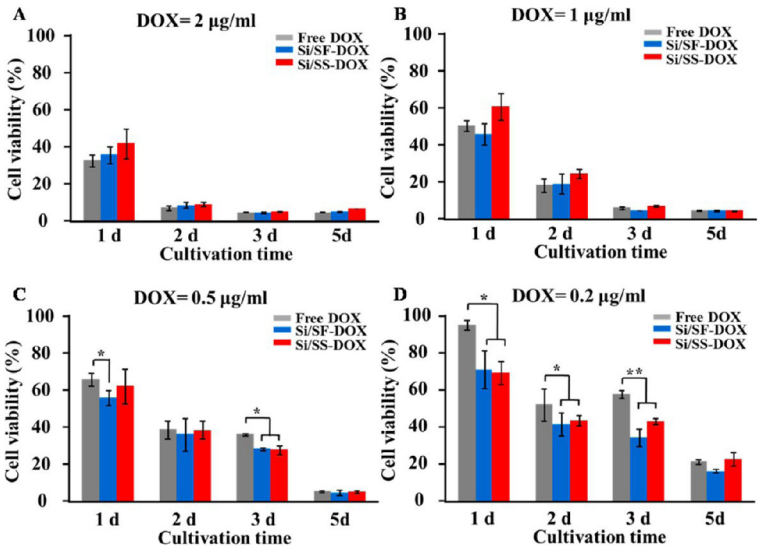

Figure 7.

Cell viability of HeLa cells after treatment with free DOX, DOX-loaded Si/SF nanospheres (Si/SF-DOX), and DOX-loaded Si/SS nanofibers (Si/SS-DOX) at varied DOX concentrations and cultured 1, 2, 3, and 5 days. The concentration of DOX treatment was set at (A) 2, (B) 1, (C) 0.5, and (D) 0.2 μg/mL.